J Vis (2010) 13:25–32
DOI 10.1007/s12650-009-0008-3

REGULAR PAPER

Hyoung Jin Lee · Bok Jik Lee · Sung Don Kim · In-Seuck Jeung

Investigation of the pseudo-shock wave in a two-dimensional supersonic inlet

Received: 16 February 2009 / Revised: 17 July 2009 / Accepted: 1 September 2009 / Published online: 12 December 2009

Abstract This paper describes experimental and numerical investigations into the multiple shock waves/turbulent boundary layer interaction in a supersonic inlet. The test model has a rectangular shape with an asymmetric subsonic diffuser of 5°. Experiments were conducted to obtain the visualization images and static pressure data by using supersonic wind tunnel. Numerical simulation was performed by solving the RANS equations with the Menter's SST turbulent model. The inflow condition was a free-stream Mach number of 2.5 and a unit Reynolds number of 7.6×10^7/m. Numerical results showed good agreement with the experimental results. Based on this agreement, the flow characteristics which are often very difficult to obtain experimentally alone were analyzed with the aid of numerical simulation. The structures, pressure and velocity distributions, and total pressure loss of the pseudo-shock wave in the supersonic inlet were presented in detail from flow visualization images and static pressures.

Keywords Visualization · Supersonic inlet · Asymmetric diffuser · Shock train · Pseudo-shock wave

1 Introduction

The pseudo-shock wave (PSW) is a complex phenomenon that is frequently observed as the result of shock boundary layer interactions (SBLIs) when a supersonic flow is decelerated to a subsonic flow in a duct. This PSW exists in a variety of fluid devices, such as diffusers of supersonic wind tunnels and scramjet engine/combustor isolators, which strongly affect their performance and efficiency. A supersonic inlet also functions to provide a subsonic flow at the desired velocity to the combustor, by decreasing the entering supersonic flow, while minimizing the total pressure loss. The overall compression process in the supersonic inlet is made up of three stages: supersonic compression by external shocks; deceleration from supersonic to subsonic with a normal shock; and the subsequent subsonic compression. The normal shock mentioned above in a supersonic inlet is usually called a terminal shock. The simplest realization of the terminal shock

H. J. Lee
School of Mechanical and Aerospace Engineering, Seoul National University, Seoul 151-742, Korea

B. J. Lee
PGM R&D Lab., LIG Nex1, Daejeon 305-804, Korea

S. D. Kim
Aerospace and Automotive Division, Hanwha corporation, Chungnam 336-871, Korea

I.-S. Jeung (✉)
Department of Aerospace Engineering, Institute of Advanced Aerospace Technology, Seoul National University, Seoul 151-742, Korea
E-mail: enjis@snu.ac.kr

is a single normal shock, but such a simple pattern rarely occurs for a higher Mach number. When the Mach number immediately upstream of the terminal shock is higher than about 1.3, the boundary layer on the wall surface of the inlet interacts with the terminal shock, which creates a PSW (Sajben et al. 1985). When a supersonic inlet is operated at the stable condition wherein the terminal shock is located in a subsonic diffuser, the most important flow feature is the PSW, their detailed forms of which depend on the structure of the shock system of the inlet. The performance and stability of the supersonic inlet are also strongly affected by the structure and location of this terminal shock. Therefore, it is very important to observe the PSW that can prevail inside the inlet.

Many previous investigations of PSWs were conducted in constant-area channels where the effects that are associated with a sustained post-shock pressure-gradient are either totally absent or greatly suppressed (Sun et al. 2003; Matsuo et al. 1999; Chyu et al. 1989; Hamed and Shang 1991; Waltrup and Billig 1973; Curran et al. 1996; Sugiyama et al. 1998). However, the phenomenon of PSWs in asymmetrically diverging diffusers of supersonic inlets is different from that in constant-area channels. For this reason, even though there are several studies of the PSW, only a few of the results are directly applicable to inlet flows. Several experimental and numerical studies of the flow in a supersonic inlet have been conducted (Talcott and Kumar 1985; Chyu et al. 1989; Hamed and Shang 1991; Sajben et al. 1992). However, most of those results focused on the unsteadiness of the terminal shock and did not clearly visualize the structure of PSWs inside the inlet.

This study was conducted to observe structures of the PSW in the two-dimensional supersonic inlet and to understand the effect of the PSW on the total pressure of the supersonic inlet system. Investigations were based on experiments that were conducted in a conventional, blow-down, supersonic wind tunnel of the Aerospace Propulsion and Combustion Laboratory at Seoul National University. Further, numerical simulations were also conducted for the data that could not be obtained from the experiments. In view of the research aim, a rectangular inlet model, which had self-starting characteristics at Mach 2.5, was used. Experimental data were obtained through static pressure measurement and a Schlieren and shadowgraph technique of flow visualization.

2 Experimental and numerical setup

2.1 Experimental setup

The supersonic wind tunnel used in this study, as shown in Fig. 1a, allows about 10 s of run-time. The test section is square-shaped and of size 109 × 109 mm. A two-dimensional, converging–diverging, supersonic nozzle, for which the design Mach number is 2.5, is located upstream of the test section. The unit Reynolds number is 7.6×10^7/m.

The inlet model is of the rectangular type, and the design method is based on Mahoney (1990). The model is a generic, mixed-compression inlet, with a cowl-lip height of about 13 mm, as shown in Fig. 1c.

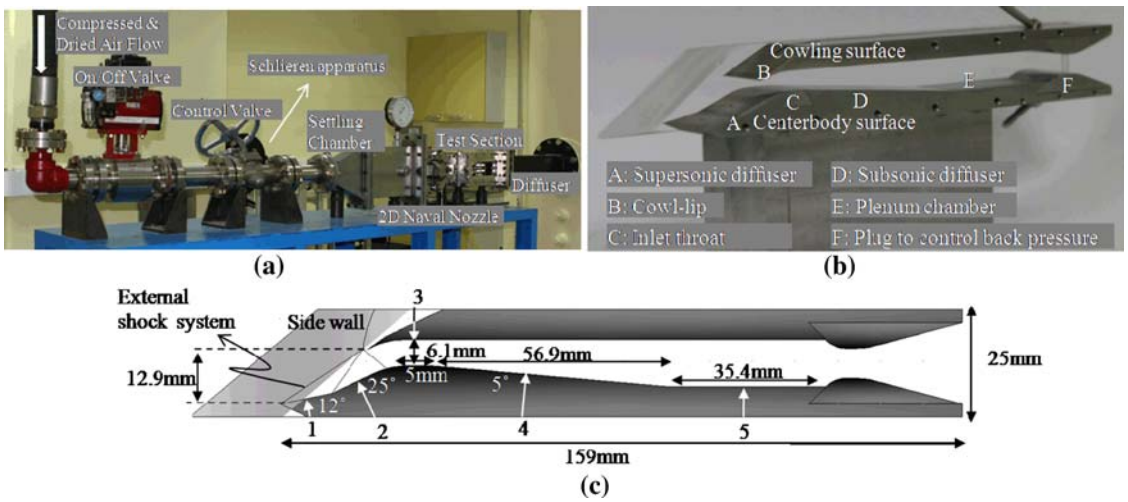

Fig. 1 Experimental apparatus. **a** Supersonic wind tunnel (SNU). **b** Picture of the inlet model. **c** Schematic of inlet test model

The test model has two fixed ramps on the centerbody; it does not use a bleeding system. The two ramp angles are decided on the basis of the maximization of the total pressure recovery through theoretical, one-dimensional calculations, under the assumption that the inlet has two oblique shocks and one normal shock. The inlet throat height was designed to be 6.1 mm, the throat length was 5 mm, the angle of the subsonic diffuser was 5°, and the total length was 159 mm. The width of the rectangular model was 20 mm. To visualize the internal flow of the inlet, Plexiglas was used for the pair of sidewalls. The stations 1–5 are the positions for measuring the static pressure. The pressure was measured by a conventional pressure transducer of the strain-gauge type. Figure 1b is a picture of the inlet test model.

Shadow and Schlieren flow-visualization is a well-established technique that is used to capture the formation of external and internal shocks of the inlet. A Z-type, four-mirrored system (Settles 2001), was used to obtain the focal distance from the continuous (Xenon lamp) or pulsed laser (Nd:YAG, 535 nm) light source to the concave mirror. Flow visualization pictures were taken by a digital CCD camera (EOS 20D, Cannon), which had a shutter speed of 1/8,000 s.

The downstream conditions were varied by changing the position of the back-plug, which controlled the throat-area of the exit jet; see part F (the plug) of Fig. 1b. The position of the back-plug identifies the area-ratio (AR), which is defined as the ratio of the geometrical throat-area of the exit jet (A_e), to the cross-sectional area at the throat section of the inlet (A_t). Experimental results were suggested for the four cases of AR wherein the terminal shock is located inside the inlet duct.

2.2 Numerical method

Using the Reynolds Averaged Navier–Stokes (RANS) equations with the Menter's shear stress transport (SST) turbulent model, numerical simulations were conducted to aid the analysis of the PSW in the supersonic inlet. Two-dimensional analysis was conducted to confirm the basic phenomenon and reduce the computational cost. The equations were solved by the well-known Jacobi iterative implicit time-marching scheme and Roe's flux difference splitting (FDS) scheme with spatial-accuracy up to the third-order by the use of the gradient limiter of Osher-Chakravathy.

The inflow boundary conditions were specified as the unperturbed, freestream conditions and were completely specified for the duration of the solution procedure. Since all the test cases were for a supersonic freestream, the fixed upstream boundary condition was adopted. For the outflow boundary condition, a no-gradient extrapolation was set at the exit due to the supersonic flow downstream of the physical flow plug that was used in the experiments. The boundary conditions for walls, such as the wall of the centerbody and the cowl surface, were treated as no-slip by setting the velocity components on the walls to zero and the adiabatic condition.

The total number of grids was about 340,000. For best results, the first cell centers from the wall were located well within the laminar sub-layer ($y+ \sim 1$). Therefore, very fine grids were located near wall-boundaries, which comprised 180 points in the transverse directions of the walls.

3 Results and discussion

3.1 Structure of the pseudo-shock wave in the supersonic inlet

Figure 2 shows the experimental and numerical results of PSW inside the supersonic inlet test model at AR = 1.156. The flow is from left to right. Figure 2a–c is the experimental shadow and Schlieren images that use a continuous light source and the numerical Schlieren image, respectively. In the numerical Schlieren image of Fig. 2c, the iso-curve that corresponds to a local Mach number of unity, from which we can distinguish between supersonic and subsonic regions, is indicated. The density-contours image that is obtained by numerical simulation is shown in Fig. 2d. The numerical results in this paper are instantaneous data for the unsteady phenomenon of the PSW. However, its oscillation was very small, and the fluctuations of static pressures were also very weak. Thus, it is thought that the instant numerical results represent sufficiently the phenomenon.

As seen from Fig. 2, the experimental and numerical results agree relatively well with each other, except with regard to the distances between consecutive shocks. From Fig. 2, we can observe the general flow characteristics of the supersonic inlet quite well, including the external shock system and the internal PSW inside the inlet model. We can clearly observe the first shock wave that is asymmetric and λ-shaped with a vertical portion (Fig. 2a, b) and two points of bifurcation, as well as the consecutive shock waves that are

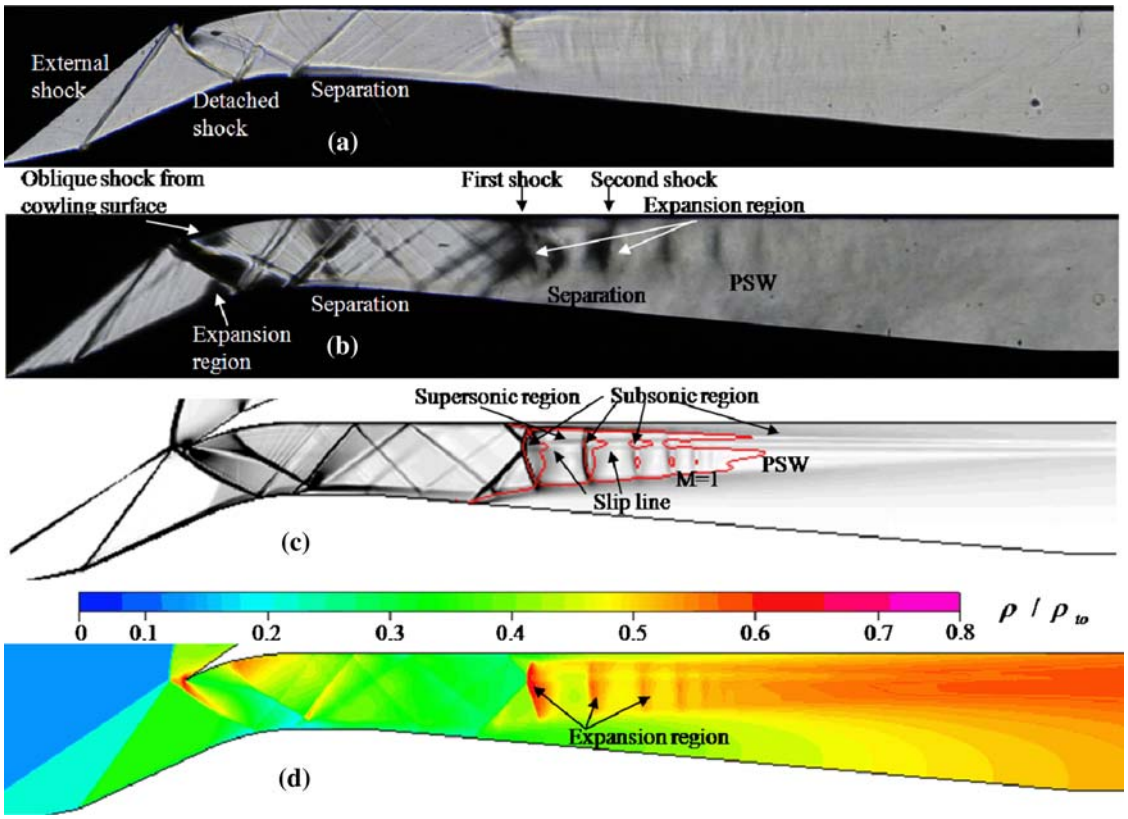

Fig. 2 Experimental and numerical results of PSW inside supersonic inlet (AR = 1.156). **a** Shadow image. **b** Schlieren image. **c** Numerical Schlieren image. **d** Numerical density contour

concave in the upstream direction (Fig. 2b, c). The boundary layer separates from the wall at the foot of the front leg of the first shock wave. In contrast to the prior results on constant-area channels (Sun et al. 2003), asymmetric oblique shocks are generated from asymmetric separation regions and a distorted diamond-shaped expansion region (Fig. 2b, d) exists immediately behind the normal part and rear leg of the first shock. These consecutive structures compose the asymmetric shock train in the subsonic diffuser. The spaces between successive shock waves and the size of the expansion region behind each shock wave gradually decrease in the downstream direction.

3.2 Terminal shock images for varying area ratios

Figure 3 shows the terminal shock (white arrows) for various area ratios. When the area ratio is relatively high, such as 1.156 and 1.090, the terminal shock develops into a PSW, and the PSW moves upstream as the area ratio decreases. As the area ratio decreases, the number of normal shocks, the spacing between consecutive shocks, and the length of shock train decreases gradually. When the area-ratio decreases to 1.025, the terminal shock moves to the inlet throat and is formed into a single normal shock at first. However, the boundary layer is much thicker at the centerbody of the inlet throat as the terminal normal shock intersects with the oblique shock that originates from the cowl-lip. Therefore, the flow passage narrows; the subsonic flow is again immediately reaccelerated to supersonic flow, and another shock train is generated. The numerical results agreed well with experimental results for all area ratios.

3.3 Static pressure distribution of the pseudo-shock wave in supersonic inlet

Figure 4 shows the static pressure distributions along the inlet duct, as obtained from the experiment and the numerical simulation, and the static pressure contours of the inlet test model at AR = 1.156. The red and green lines represent the static pressure of the numerical results along the centerbody and cowling surface,

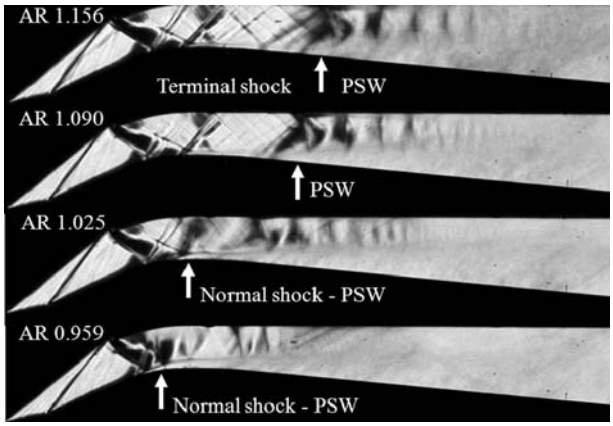

Fig. 3 Terminal shock images for various AR

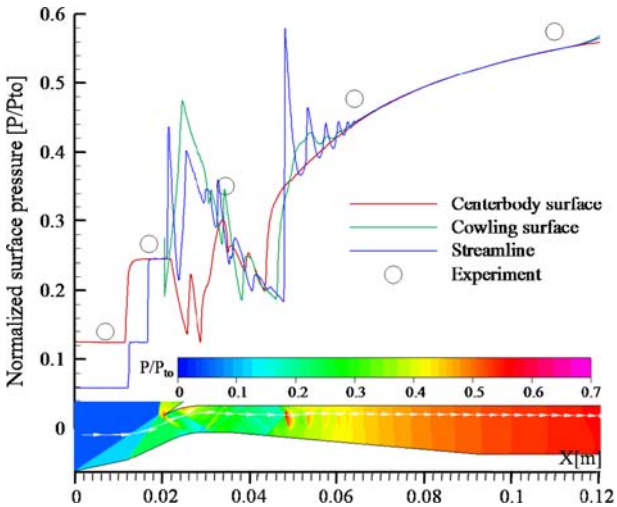

Fig. 4 Static pressure distribution and pressure contours

respectively. The blue line represents the local pressure along the streamline that is denoted in the pressure-contour in Fig. 4. The open circles represent the experimental results. The horizontal axis denotes the distance (X) from the tip of the first ramp, and the vertical axis represents the static pressure (P), normalized by the stagnation pressure (Pto), in the upstream settling chamber. Figure 4 indicates that the experimental result on the wall pressure is slightly higher than the numerical result. The reason for this may be faults in the turbulence model used in this study and the three-dimensional effect of the small-sized test model. However, the results are sufficient to explain the phenomena of PSW inside the inlet test model. Figure 4 shows the pressure rise that is induced by the PSW inside the inlet. Most of the pressure rise occurs at the first leading shock and then continues to rise rather moderately, although there is a jagged pressure along the cowling surface and the streamline after the first leading shock. Also, similar to the prior results on PSWs in constant-area channels (Matsuo et al. 1999; Sun et al. 2003), remarkable fluctuations in the pressure are observed along the normal shock part of the PSW of the streamline. The curves of the static pressure distribution along the streamline of the test model show that the pressure increase due to the first shock is larger and steeper than that due to the successive shocks, as with the results for the constant-area channel. However, the steep pressure rise occurs on the centerbody surface, cowling surface, and streamline in that order, while the steep rises occur at the same position on the centerbody and cowling surface for the constant-area channels (Sun et al. 2003), i.e., caused by the asymmetric normal shock train, as shown in Figs. 2 and 3.

Static pressure distributions of the centerbody surface still preserve a smooth and stable trend of growth but those of the cowling surface fluctuate slightly; these fluctuations are caused by asymmetric shock trains. The shape of the shock train is related to the thickness of the boundary layer that develops at the subsonic diffuser. The oblique shock that is generated from the cowl-lip is reflected at the centerbody surface of the inlet throat, which greatly thickens the boundary layer at the centerbody surface. On the other hand, the boundary layer that develops on the cowling surface is a lot thinner because no major factors can thicken the boundary layer at this surface as the external oblique shocks are located outside the cowl-lip. This asymmetrically distributed boundary layer is the main cause of the asymmetric shock train at the subsonic diffuser. In this asymmetric shock train, distinct differences exist between the two bifurcating oblique shocks in terms of: the originating position of the shock; the shock length; and the shock strength. The oblique shock on the centerbody is longer and stronger than that on the cowling surface, which makes the boundary layer near the centerbody surface even thicker and thereby results in a smooth surface-pressure distribution, as shown in Fig. 4. In contrast, because the supersonic core flow is obviously deflected to the cowling surface, the surface pressures on this side are easily affected by shock waves and expansion waves in the shock train, and exhibit pressure fluctuations in the streamwise direction. As to the flow region following the shock train, the dominant flow processes are supersonic mixing and subsonic diffusing; therefore, the surface-pressure distribution of the cowling surface reverts to a smooth trend and agrees with that of the centerbody surface.

3.4 Velocity distribution of the pseudo-shock wave in the supersonic inlet

Figure 5 shows the Mach number contours and the velocity vector distribution from the numerical result at AR = 1.156. Figure 5a is the Schlieren image that is obtained from a continuous Xenon lamp whose exposure time is determined from the shutter speed of the camera, viz, 1/8,000 s. Figure 5b is the shadow image that is obtained through pulsed laser beam whose exposure time is 5–7 ns. The shape of shocks, the separation region, and the boundary layer are observed more clearly from Fig. 5b. As shown in Fig. 5b, e, the boundary layer separates at the foot of the front leg of the first shock. A large reverse-flow region can be

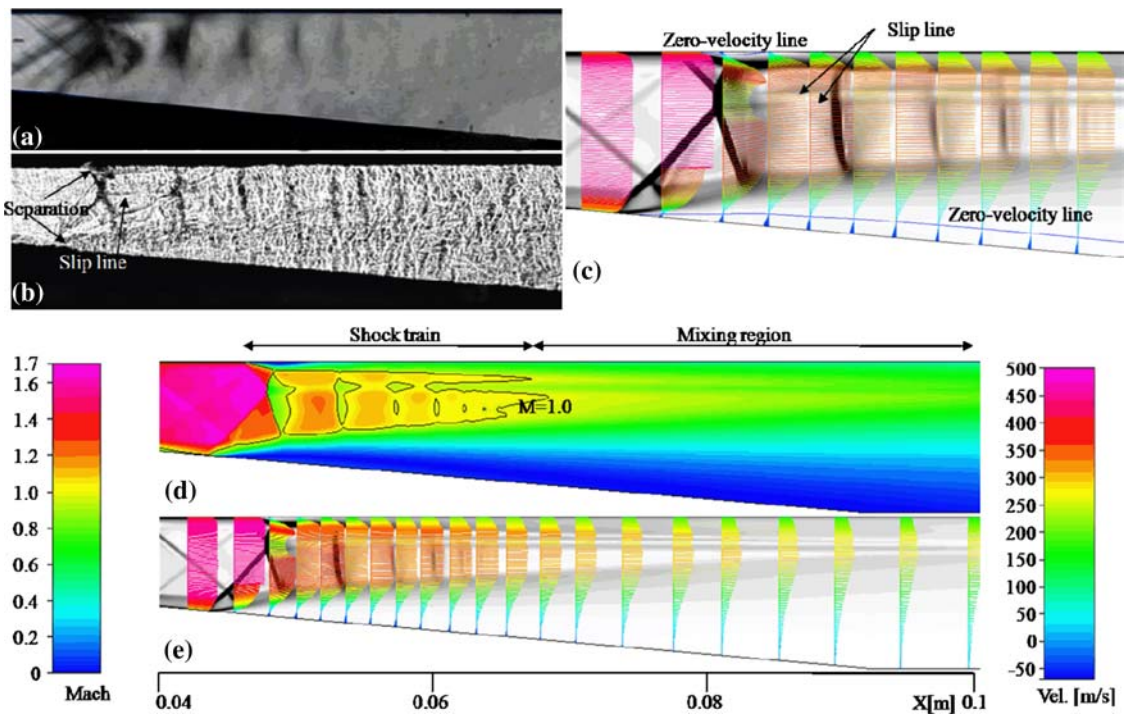

Fig. 5 Detailed visualization images and Mach number and velocity vector distribution of the PSW. **a** Schlieren image using continuous light source (exposure time 125 μs). **b** Shadow image using laser light source (exposure time 5–7 μs). **c** Detailed velocity distribution around the shock train

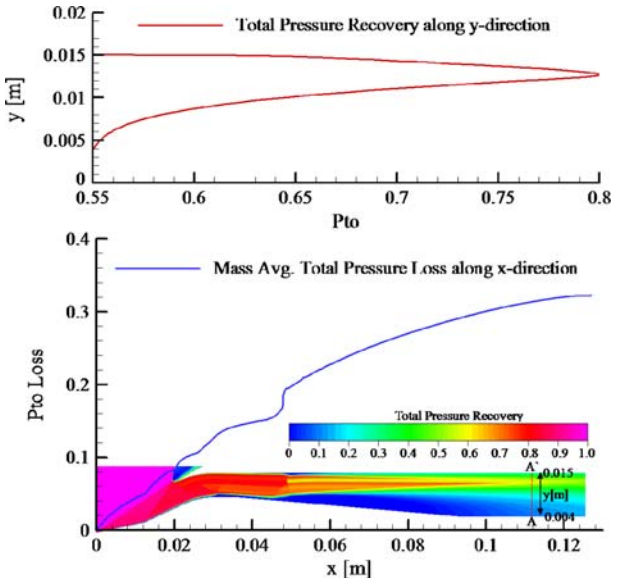

Fig. 6 Total pressure parameters in the PSW inside the inlet

found under the zero-velocity line near the wall, and a recirculation appears between the rear leg of the first shock and the duct wall. A large increase in the boundary layer thickness is observed passing through the front legs on the centerbody, which results in an asymmetric shock train, and the core flow is formed on the cowling surface. However, the general features are similar to those of PSWs in constant-area channels except for this asymmetry. Since the velocity of the normal shock part is lower than that of the oblique shock parts, two weak slip lines emanates from the bifurcation points in the downstream direction (Fig. 5b, c). The region between these two slip lines is the slowest at the cross-section of the shock train region, and therefore, the velocity profile is saddle-shaped. The core flow behind each shock becomes subsonic and then accelerates again to supersonic before the next shock appears as shown in Fig. 5c. The flow just behind the shock train is mixed supersonic near the outer edge of the boundary layer (supersonic tongue) and subsonic in the core region. In the mixing region, as the low-speed flow extends to the center of the core flow, the entire flow gradually decelerates to subsonic. Therefore, the velocity profiles change from trapezoidal behind the shock train to parabolic in the mixing region.

Figure 6 shows the typical characteristics of the total pressure parameters in the PSW of the supersonic inlet, which are estimated from the numerical solution. The blue line represents the mass-averaged total pressure loss ratio along the x-direction. The red line is the local total pressure recovery along the y-direction at the cross-section, which is denoted by a red line, A–A′, in the plenum chamber of the local total pressure recovery contours. The local total pressure recovery is defined as the ratio of the local total pressure to the inflow total pressure. The mass-averaged total pressure recovery, η_{P_t}, and the loss ratio, $\eta_{P_{t\_l}}$, are estimated with the following definition,

$$\eta_{P_t} = \frac{\int_A \rho u P_t \mathrm{d}A \Big/ \int_A \rho u \mathrm{d}A}{\int_{A_i} \rho u P_t \mathrm{d}A_i \Big/ \int_{A_i} \rho u \mathrm{d}A_i}$$

$$\eta_{P_{t\_l}} = 1 - \eta_{P_t}$$

where ρ, u, A, and A_i are the local density, the local velocity, the section area at any x, and the section area at the entrance of the inlet, respectively. The mass-averaged parameters mean that the total pressure is weighted by the local mass flux and integrated over the section. The mass-averaged total pressure loss continuously increases in all the regions, but its severe spike is generated at the leading normal shock portion, which is precisely the point of bifurcation. Another jump in the total pressure loss is not observed in the succeeding normal shock that lies behind the leading normal shock. In the PSW region, about 20% of the total pressure loss is generated at the first normal-shock portion. The local total pressure recovery at the

plenum chamber is distorted, because the core flow is deflected to cowl surface due to the asymmetric PSW in the subsonic diffuser of the inlet. The value is higher along the flow passage, where the core flow is formed, because the local velocity is high through this passage.

4 Conclusion

Experiments to observe the PSW in the asymmetric diffuser of a two-dimensional supersonic inlet were conducted in a supersonic wind tunnel at Mach 2.5. Numerical simulation was also performed on the basis of two-dimensional RANS equations by using a Menter's SST turbulence model. The two set of results agree relatively well with each other. Based on these investigations, the structures, pressure and velocity distributions and the total pressure recovery of the PSW are analyzed in detail.

1. In contrast to the prior results on PSWs in constant-area channels, an asymmetric PSW is observed. Although the PSW that is observed inside the inlet is asymmetric, the structure of the PSW is similar to that of PSWs in constant-area channels. We can observe the first shock wave that is λ-shaped, the two points of bifurcation, and succession of concave shock waves. However, because of the asymmetry, a distorted diamond-shaped expansion exists immediately behind the normal part and the rear leg of the first shock, unlike the structure of the PSW in constant-area channels.
2. The boundary layer is distributed asymmetrically due to the effect of the reflected external shock system and the geometry of the asymmetric diffuser. The asymmetric PSW is formed from this asymmetrically distributed boundary layer. The boundary layer separates from the wall at the first shock wave; then, it is considerably thicker on the centerbody surface, which results in a core flow that is deflected to the cowl-side. Owing to this deflection of the core flow, the static pressure distributions of the centerbody surface still preserve a smooth upward trend, but those of the cowling surface exhibit considerable fluctuations.
3. The local total pressure recovery in the plenum chamber is higher along the flow passage, where the core flow is formed, because the local velocity is high through the passage. The mass-averaged total pressure loss continuously increases in all the regions of the PSW, but its severe spike is generated at the leading normal-shock part and is about 20% of the total pressure loss in the PSW.

Acknowledgments This work was supported by the Defense Acquisition Program Administration and the Agency for Defense Development under the contract UD070041AD, and KOSEF grant funded by the Korea government (MEST).

References

Chyu WJ, Kawamura T, Bencze DP (1989) Navier-Stokes solutions for mixed compression axisymmetric inlet flow with terminal shock. J Propuls Power 5–1:4–5

Curran ET, Heiser WH, Pratt DT (1996) Fluid phenomena in scramjet combustion systems. Annu Rev Fluid Mech 28:323–360

Hamed A, Shang JS (1991) Survey of validation data base for shock wave boundary layer interactions in supersonic inlets. J Propuls Power 7–4:617–625

Mahoney JJ (1990) Inlets for supersonic missiles. AIAA education series, pp 55–66

Matsuo K, Sasaguchi K, Mochizuki H, Takechi N (1980) Investigation of the starting process of a supersonic wind tunnel. Bull JSME 23–186:1975–1981

Matsuo K, Miyazato Y, Kim HD (1999) Shock train and pseudo-shock phenomena in internal gas flows. Prog Aerosp Sci 35(1):33–100

Sajben M, Bogar TJ, Kroutil JC (1985) Experimental study of flows in a two-dimensional inlet model. J Propuls Power 1–2:109–117

Sajben M, Donovan JF, Morris MJ (1992) Experimental investigation of terminal shock sensors for mixed-compression inlets. J Propuls Power 8–1:168–174

Settles GS (2001) Schlieren and Shadowgraph techniques. Springer, Berlin, pp 42–48

Sugiyama H, Arai T, Kagawa K (1998) Multiple shock wave/turbulent boundary layer interaction and turbulence phenomena in a supersonic rectangular duct. In: Proceedings of 4th KSME-JSME fluids engineering conference, pp 25–28

Sun LQ, Sugiyama H, Mizobata K, Fukuda K (2003) Numerical and experimental investigations on the Mach 2 pseudo-shock wave in a square duct. J Vis 6–4:363–370

Talcott NA Jr, Kumar A (1985) Two-dimensional viscous simulation of inlet/diffuser flows with terminal shocks. J Propuls Power 1–2:103–108

Waltrup PJ, Billig FS (1973) Prediction of pre-combustion wall pressure distributions in scramjet engines. J Spacecr Rockets 9:620–622